Pergamon

Int. J. Heat Mass Transfer. Vol. 40, No. 14, pp. 3361–3373, 1997
© 1997 Elsevier Science Ltd. All rights reserved
Printed in Great Britain
0017–9310/97 $17.00+0.00

PII: S0017–9310(96)00369–9

A generalized thermal modeling for laser drilling process—II. Numerical simulation and results

R. K. GANESH and A. FAGHRI†
Mechanical Engineering Department, The University of Connecticut, Storrs, CT 06269-3139, U.S.A.

and

Y. HAHN

Physics Department, The University of Connecticut, Storrs, CT 06269-3046, U.S.A.

(*Received* 7 *March* 1996 *and in final form* 29 *October* 1996)

Abstract—Once the fluid configuration and the associated velocity field are obtained in a given time step using the VOF method which tracks the free surface, the energy equation is solved as an advection–diffusion equation using the control volume finite difference method. The energy equation rigorously models the phase-change both ways and tracks down the phase front as well. This paper discusses the verification of the phase-change model in cylindrical coordinates with the available results in the literature for a two-region freezing problem and its subsequent incorporation into the laser drilling model making the phase-change submodel robust in many respects. Numerical material removal rates are compared with experimental ones and found to be in good agreement. Contour plots of solid, fluid, pressure and temperature are provided at different times during the drilling process. © 1997 Elsevier Science Ltd.

1. INTRODUCTION

The fractional volume of fluid [1] method preserves the free surface of the liquid which a standard finite difference method cannot. While the pressure and the velocity components are obtained in an implicit manner, the free surface tracking is carried out explicitly obeying certain donor–acceptor fluxing rules. The time step is decided either by the viscous limit or the convection limit depending upon whichever is lower. The fluid is not allowed to convect more than half the cell width in a time step using the limited compressibility option. The placement of the field variables in the VOF method is exactly identical to that of the control volume finite difference method [2]. Whereas the VOF method uses the conservation equations in the cylindrical coordinates formulation (for the laser drilling simulation) and a combination of donor-cell and finite difference discretization approaches, the finite difference control volume approach integrates the differential equation over each control volume. The staggered grid arrangement is used for the location of velocity components and pressure both in the stand alone phase-change verification problem (control volume approach) and in the laser drilling simulation (VOF approach). For the same identical computational grid in the r–z plane, common to both methods, the VOF method has the thickness built into the governing differential equations (in cylindrical coordinates) themselves, whereas the control volume method has it calculated explicitly [3]. The common grid computational domain approach makes it possible to adopt the solution strategy of solving the isothermal hydrodynamical equations first for the velocity and pressure fields and then the energy equation for the temperature field and the location of the phase-front. The energy equation has been transformed into a nonlinear equation with a single dependent variable [4]. The nonlinearity of the phase-change problem is due to the existence of the moving phase-change front. At the solid–liquid interface at the end of the mushy region, the velocities u and v become zero. This behavior must be taken into account in the solution of the momentum equations [5, 6]. For this, a smearing approach [7] for the viscosity model which gradually increases the viscosity from that of the fluid to a very high value in the solid through the mushy zone is used to enforce the no-slip velocity boundary conditions at the solid–liquid interface. In the actual laser drilling process, the material is removed by a combination of melt ejection and vaporization, with the former being the dominant mode for lower laser intensities. In the numerical simulation process, removal by melt ejection is mim-

† Author to whom correspondence should be addressed.

NOMENCLATURE

a	coefficient in the discretization equation
c	specific heat [J/kg/K]
C	ratio of specific heats
E	experimental result
F	volume of fluid function
I	intensity of laser beam [W/m^2]
k	thermal conductivity [W/m/K]
K	ratio of thermal conductivity
L	latent heat [J/kg]
N	numerical result
p	pressure [N/m^2]
Pr	Prandtl number
S	source term in the discretization equation
Ste	Stefan number
t	time coordinate [s]
T	temperature [K]
u, v	velocities [m/s].

Greek symbols

α	thermal diffusivity [m^2/s]
δ	semi phase change temperature interval, δT^0[K]
Δ	change in quantity
ε	tolerance
ν	kinematic viscosity [m^2/s]
ρ	density [kg/m^3].

Subscripts

0	maximum
abs	absorbed
e	east
c	cold
h	hot
i	inner
l	liquid phase
m	melt
n	north
o	outer
s	solid phase
s	south
sl	solid to liquid
w	west.

icked by resetting the full or partial fluid cells (which were empty cells at the beginning and became full or partial fluid cells because of fluxing of fluid due to the radial pressure gradient) that exist just over the initial surface of the solid to empty cells. In this way, once the fluid is removed, the melt–vapor interface starts moving inward into the material. The other moving boundary which is the liquid–solid interface is tracked down by the phase-change algorithm rather implicitly using the properties of the two phases.

The advantages of the solution strategy adopted here are as follows:

(1) This method of obtaining the temperature field in two steps, particularly when the energy equation in nonlinear due to phase-change capability, reduces the solution time significantly when compared to solving it simultaneously along with the momentum and continuity equations.
(2) There is only one common fixed computational grid, to obtain the velocity and temperature fields even though they are obtained separately and sequentially.
(3) The no-slip velocity boundary conditions can be applied properly using a variable kinematic viscosity smearing technique which applies the zero velocity on the solid surface in a gradual and gentle manner.
(4) The liquid–solid phase front is obtained in a self-consistent manner without explicitly tracking the phase front. This makes the phase-change numerical model less computationally intensive without having to resort to coordinate transformation etc. and makes the extension to three-dimensional (3-D) possible in the future.

The disadvantages of this solution strategy are:

(1) Since the energy equation is solved in an implicit manner and under-relaxation of the variables is necessary to deal with the nonlinearity inherent in any phase-change modeling, it takes a significant amount of time to simulate the drilling process. However, it can be said that time is expended in favor of a better fundamental physical model.
(2) The convergence of the solution of the energy equation may be in jeopardy under certain extreme simulations, for example, high intensity drilling.

2. PHASE-CHANGE SUBMODEL VERIFICATION

The temperature transforming phase-change model was developed and tested [4] with the available results in the literature in Cartesian coordinate system. In laser drilling modeling, an axisymmetric coordinate system is better suited because of the nature of the process. Therefore, as the first step, the stand-alone temperature transforming model which was originally written for the Cartesian coordinate system has to be modified to accommodate a cylindrical coordinate system and as a second step should be verified using the available experimental and analytical results that exist in the literature. It can then be incorporated into

the two-dimensional (2-D) axisymmetric laser drilling model enhancing its phase-change submodel.

2.1. *Experimentation*

Physical experiments were performed for freezing under conditions where the liquid phase is either above or at the fusion temperature i.e. superheated or non-superheated liquid) initially [8]. Here, in this exposition the experimental data furnished in the paper [8] will be used to verify the numerical results for a freezing problem with and without the presence of natural convection. A liquid is placed at temperature T_0 in a cylindrical containment vessel whose ends are thermally insulated and whose outer surface is held fixed at temperature T_0. Freezing begins when a cooled inner cylinder at temperature T_i is inserted into the liquid at the center. This freezing in a thermal cavity is analyzed numerically. Even though natural convection is not present in the laser drilling process, for the verification of the stand alone phase-change model it has to be considered. The numerical results of both the superheated and the non-superheated simulations will be compared with the experimental ones quantitatively.

2.2. *Numerical experimentation*

The phase-change medium used in the physical experiment was n-eicosane, a paraffin phase-change material (PCM) and an unbranched alkane ($C_{20}H_{42}$) whose melting temperature T_m is about 36°C. The experimental setup is discussed in ref. [8]. The same dimensions, as used in the physical experiment were input into the stand-alone computer program to study the freezing problem. The thermophysical properties of n-eicosane were obtained from the design handbook of refs [9–11].

2.2.1. *Non-superheated liquid freezing problem.* When the liquid phase is at or above the fusion temperature before freezing commences, the condition of the liquid phase is referred to as saturated (non-superheated) or superheated, respectively. The numerical simulation of the advancement of the freezing front inside the cylindrical containment vessel was run with a computational grid comprising 40 by 76 cells in the radial and axial directions, respectively. The thermophysical properties, namely, the thermal conductivities k_l, k_s and their ratio K_{sl}, density ρ and specific heats c_l, c_s and their ratio C_{sl} and the latent heat of fusion, L for n-eicosane were used in the two-region analysis. The nondimensionalized initial and the outer temperature is 0 and the inside (cylinder) temperature is -1.0, where temperature 0 corresponds to that of melting. The control volume finite difference method as discussed previously was used. From this numerical result, the diameter of the frozen cylinder vs time is plotted against the analytically obtained result of [8] and the agreement is very good as shown in Fig. 1.

2.2.2. *Superheated liquid freezing problem.* One of the significant mechanisms of heat transfer present in the superheated case over the non-superheated case is the presence of natural convection. The frozen front in the actual experiments were observed to be contoured and smooth as opposed to straight and rough as in the non-superheated case. One other important observation is that the growth of the frozen layer is eventually stopped by the natural convection process, thereby reaching a terminal frozen thickness. The initial and the outer temperature, T_0 or T_h is 0.39 (superheated) and the inside (cylinder) temperature T_i or T_c is -0.6096. The temperature contours were obtained up to 80 min of real time simulation as shown in Fig. 2, using a sparse 20×38 cell (in the radial and axial directions, respectively) computational grid. The temperature contours compare favorably, qualitatively with those of ref. [7] who had compared his results qualitatively with the experimental results of ref. [8].

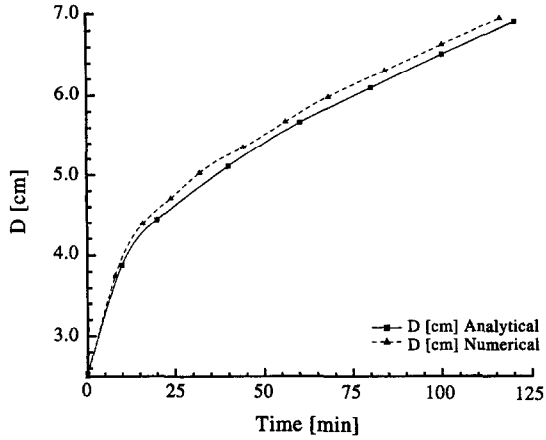

Fig. 1. Freezing front in a cylindrical tank: position of solid–liquid interface (diameter in cm) as a function of time (in minutes) for freezing in a non-superheated liquid.

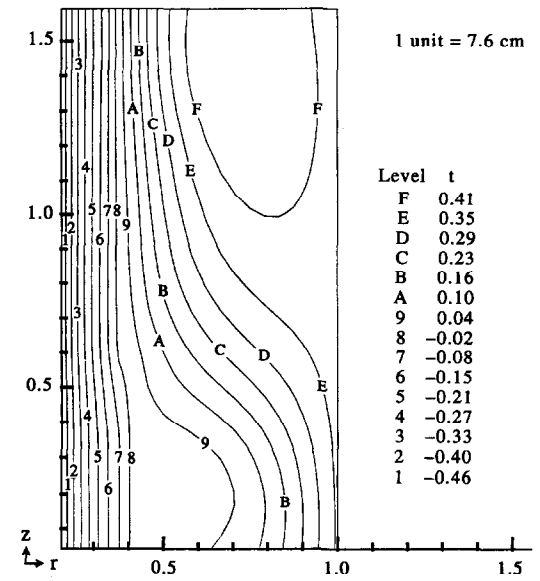

Fig. 2. Temperature contours after 80 min into the simulation: position of solid–liquid interface (contour close to 8) for two-region freezing in a super-heated liquid.

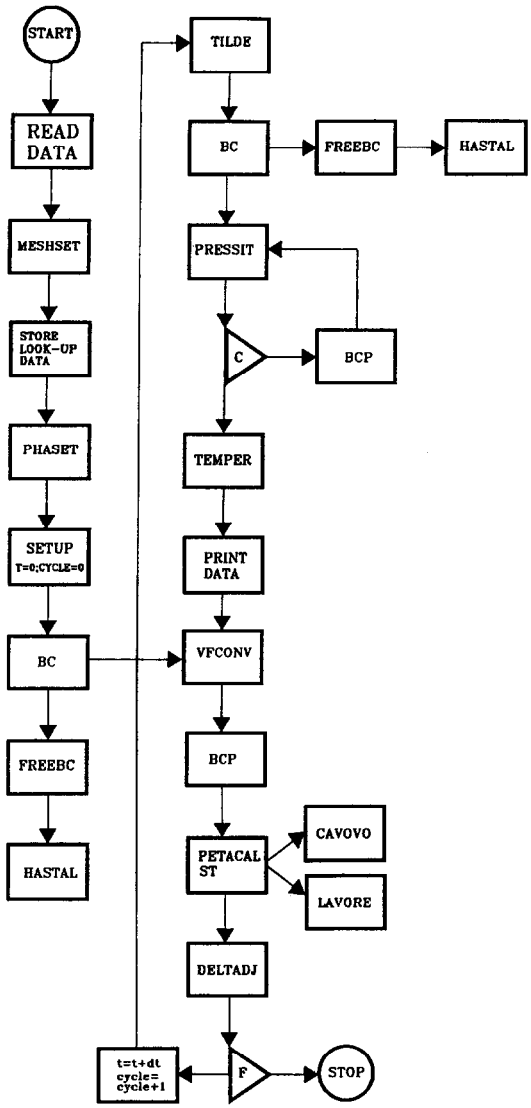

Fig. 3. Flow chart for the computer program: this program evolved from SOLA-VOF (solution algorithm for volume of fluid method).

The radius of the freezing front near the bottom of the cylinder after 30 min real time was measured to be 2.2 cm which agrees very well quantitatively with the experimentally observed radius [8] at about the same time.

2.3. *Implementation of phase-change submodel*

After the verification phase of the stand alone phase-change model in cylindrical coordinates as discussed above, only the solution algorithm for the energy equation in the phase-change model was adapted and incorporated into the computer program [12], replacing the switch-on switch-off phase-change submodel. The flow-chart for the main computer program is shown in Fig. 3. The newly introduced subroutine PHASET specifies the ratio of the thermophysical properties of the two phases, namely, K_{sl}, C_{sl}, mushy zone range δT^0, *Ste* etc. and the modified subroutine TEMPER incorporates the implicit solution algorithm for the energy equation. The velocity components obtained from VOF method are made available in the subroutine TEMPER through a COMMON BLOCK which are then used in the advection terms of the energy equation. In each time step, the previous temperature field and the newly obtained velocity field are available at the beginning of this subroutine which treats the previous temperature field as the initial temperature field for the current time step and finds the new temperature field iteratively in an implicit manner. Succinctly, the algorithm does the following in a sequential manner [4] as shown in the flow chart Fig. 4.

(1) Set counter for iteration and reset full or partial fluid cells that lie above the initial solid surface to empty cells. This mimics the melt ejection process.
(2) Searching column by column, apply constrained temperature top boundary conditions, only on fairly filled fluid cells neglecting near empty ones. The top domain boundary consists of fluid cells (inside the laser beam) as well as solid cells (outside the laser beam).
(3) Define phase-change coefficients, $C(i,j)$, $S(i,j)$ and $K(i,j)$.
(4) Calculate conductances using interface conductivity that uses the harmonic mean [2], flow rates or fluxes across the four faces using the velocity components and the discretization coefficients a_E, a_W, a_N and a_S.
(5) Apply adiabatic temperature boundary conditions on the east, wet and the south faces of the fixed grid.
(6) Obtain the relaxed temperature field using a relaxation factor of 0.1 to handle the nonlinearity using the tridiagonal matrix algorithm (TDMA).
(7) Update the phase-change coefficients using the relaxed temperature field for the two phases and the mushy zone.
(8) Repeat until another temperature residue is within the allowable tolerance or a certain number of iterations are exceeded.
(9) The new temperature field has the phase-front contained in it implicitly. Relax the temperature field with respect to the previous time step temperature field with the relaxation factor of 0.1 and obtain a new temperature field which will then be the initial temperature field for the next time step.
(10) Switch solid cells to fluid cells or *vice versa* based on the new temperature field. Mushy zone cells are fluid cells with variable viscosity.
(11) Calculate viscosity in the mushy zone using the new temperature as the key. The viscosity is set to a very large number in the solid and an expression is used in the mushy zone to make a linear transition to that of the fluid. The volume

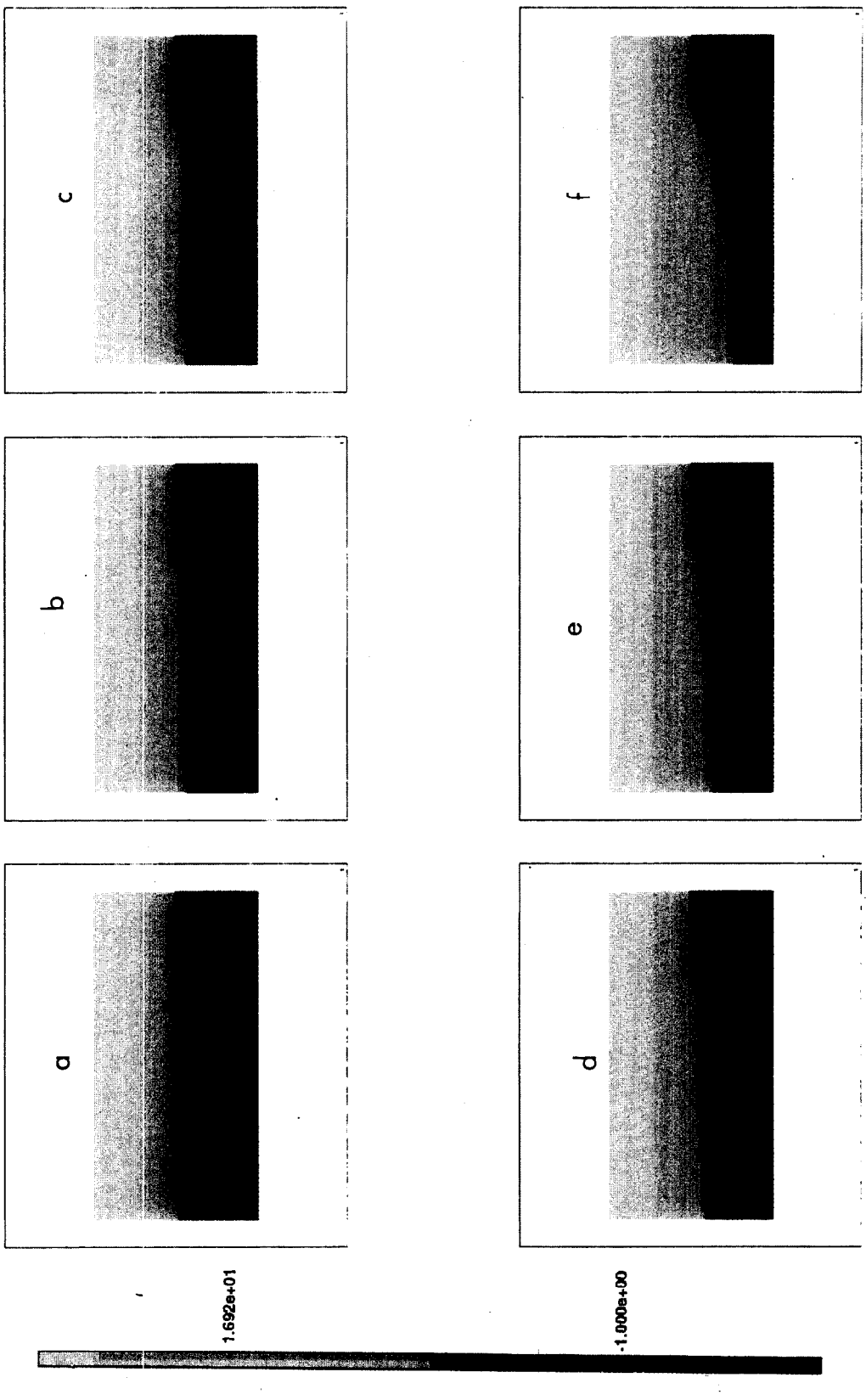

Fig. 5. Solid contours at 0 (a); 40 (b); 50 (c); 60 (d); 90 (e); and 210 (f) μs: solid cells are marked by the flag whose value is set to -1. When the value is positive the cell is either empty or a fluid.

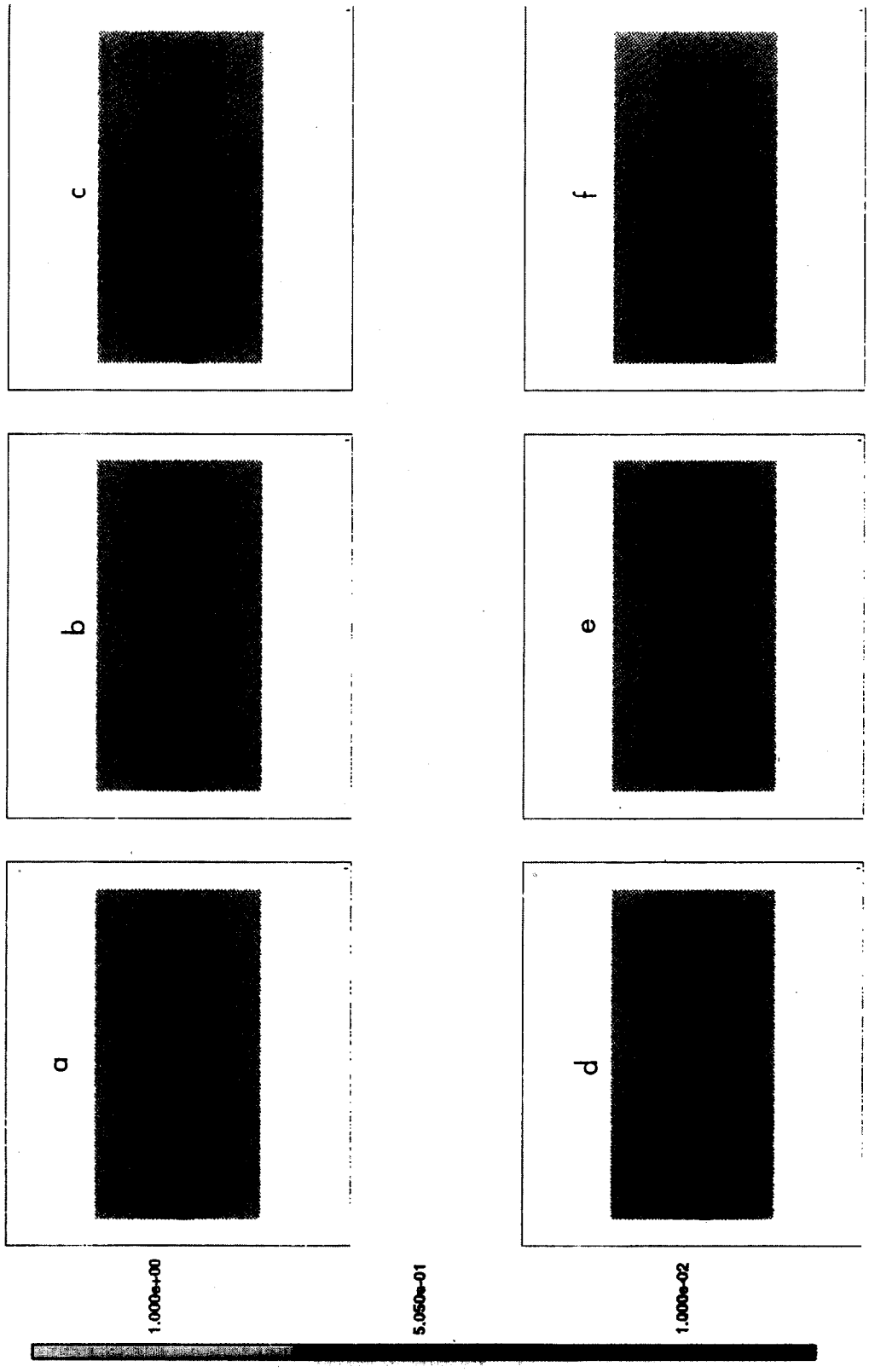

Fig. 6. Fluid contours at 0 (a); 40 (b); 50 (c); 60 (d); 90 (e); and 210 (f) μs: the fluid cells are marked by the flag whose value lies between 0 and 1. This sequence depicts the radial movement of the melt caused by the pressure gradient and its ejection.

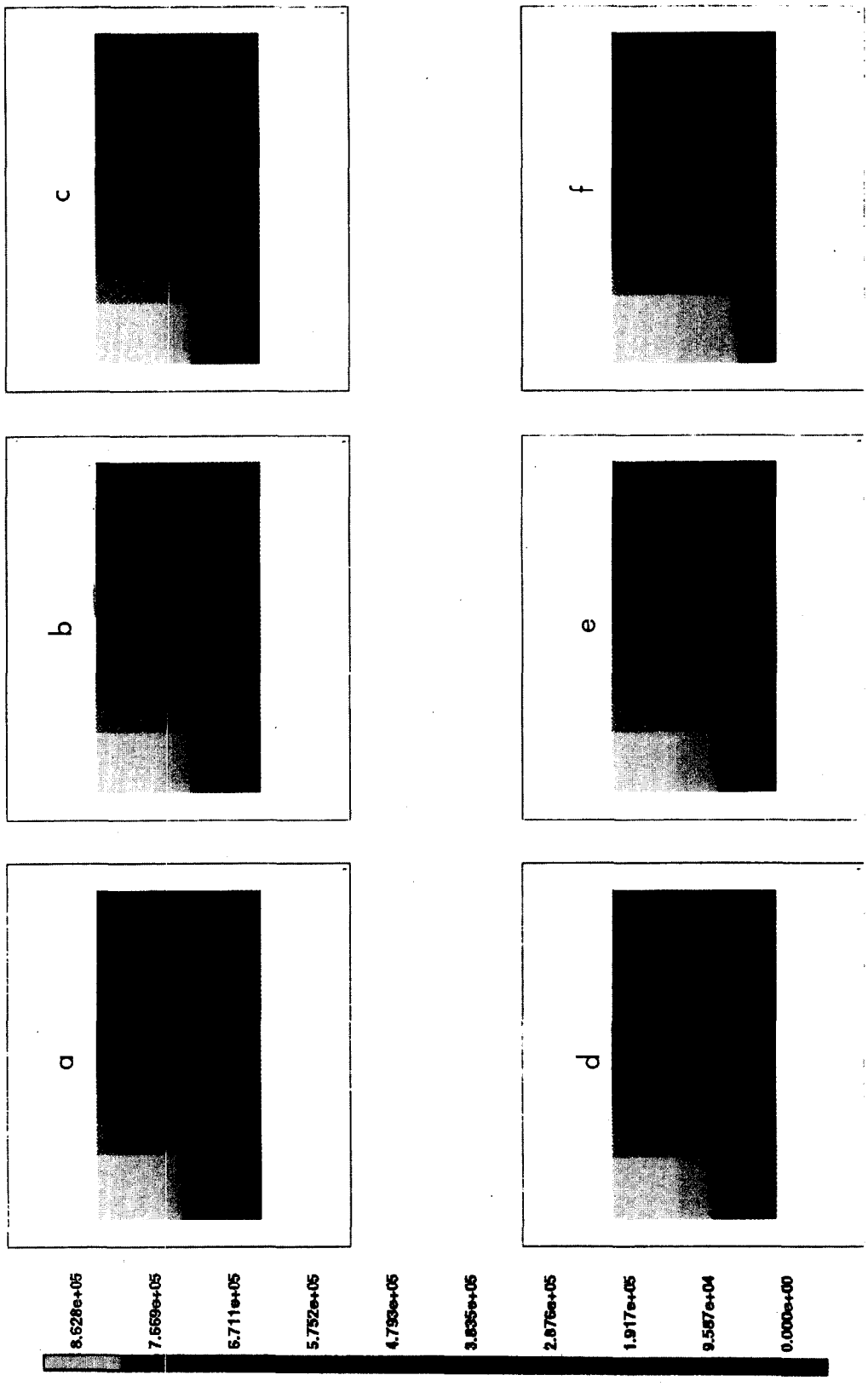

Fig. 7. Pressure contours at 0 (a); 40 (b); 50 (c); 60 (d); 90 (e); and 210 (f) μs: the pressure (nondimensionalized) is applied column-wise and is impressed on the melt's free surface. The radial gradient is depicted clearly with the maximum along the axis.

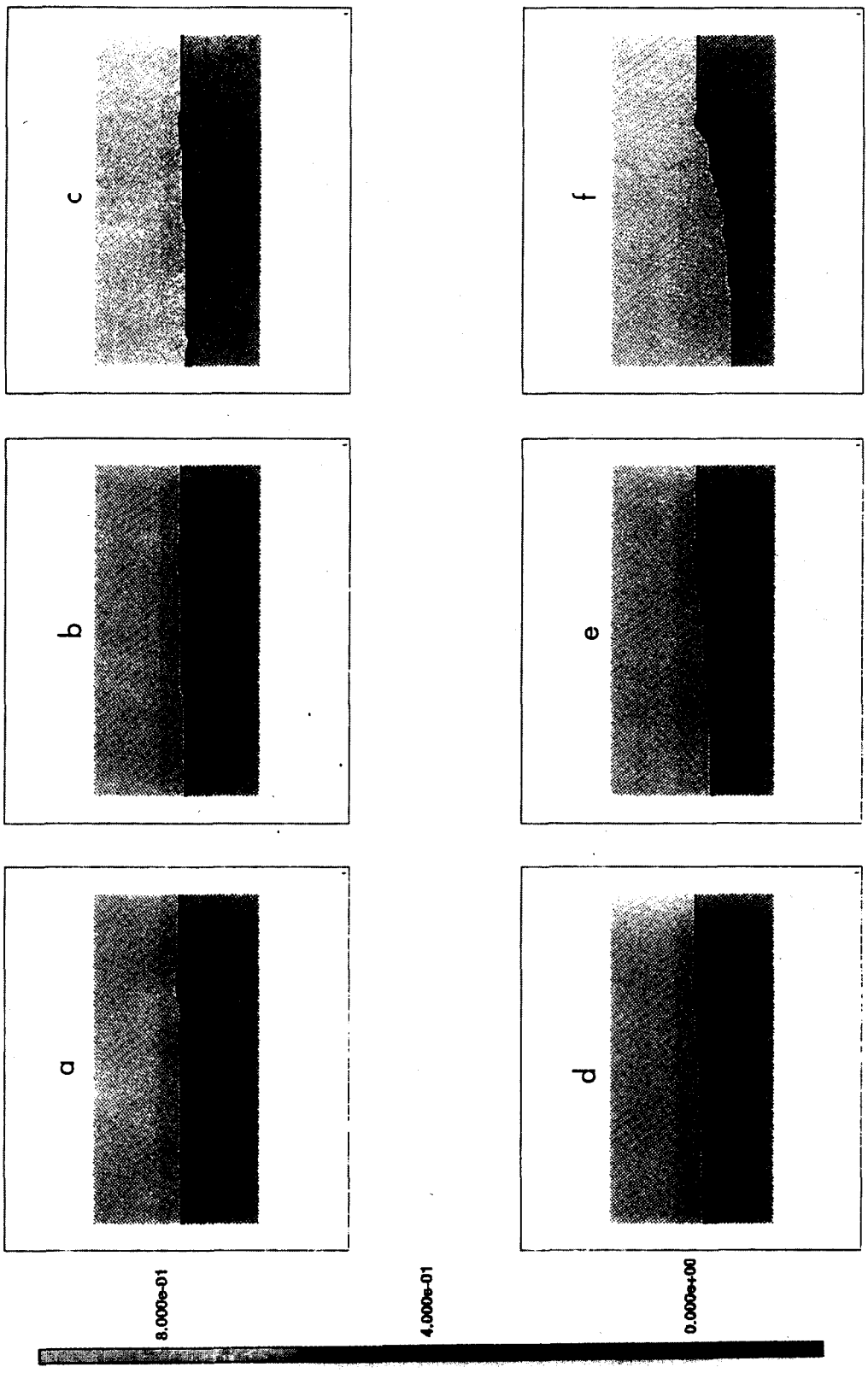

Fig. 8. Temperature contours at 10 (a); 40 (b); 50 (c); 60 (d); 90 (e); and 210 (f) μs: the temperature (nondimensionalized) is shown between 0 (melting point) and 0.7. The melt layer is thin as the melt front advances in to the solid due to melt ejection.

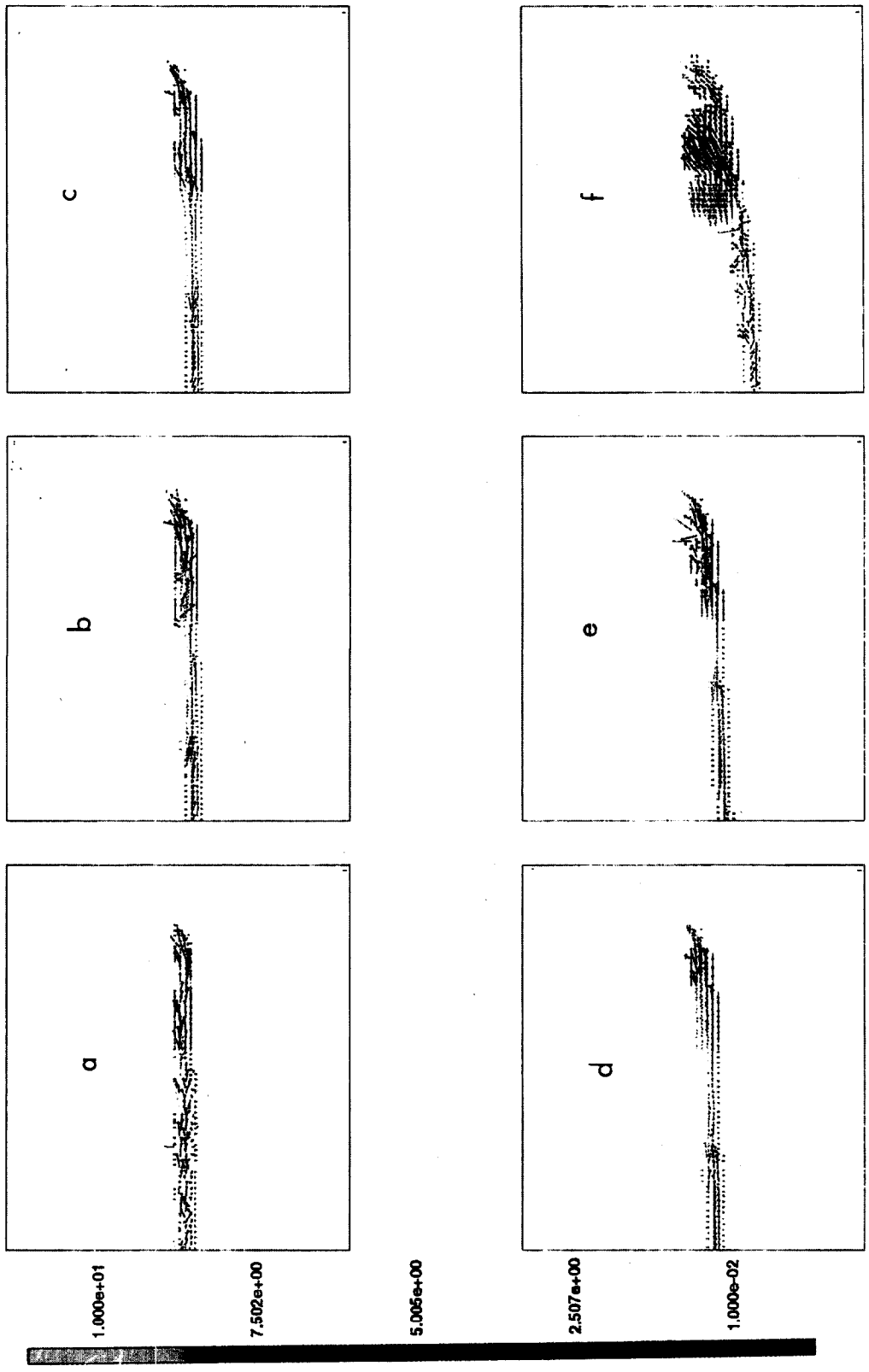

Fig. 9. Velocity vectors at 10 (a); 40 (b); 50 (c); 60 (d); 90 (e); and 210 (f) μs: the vectors (nondimensionalized) range from 1 to 10. The radial movement and ejection are portrayed.

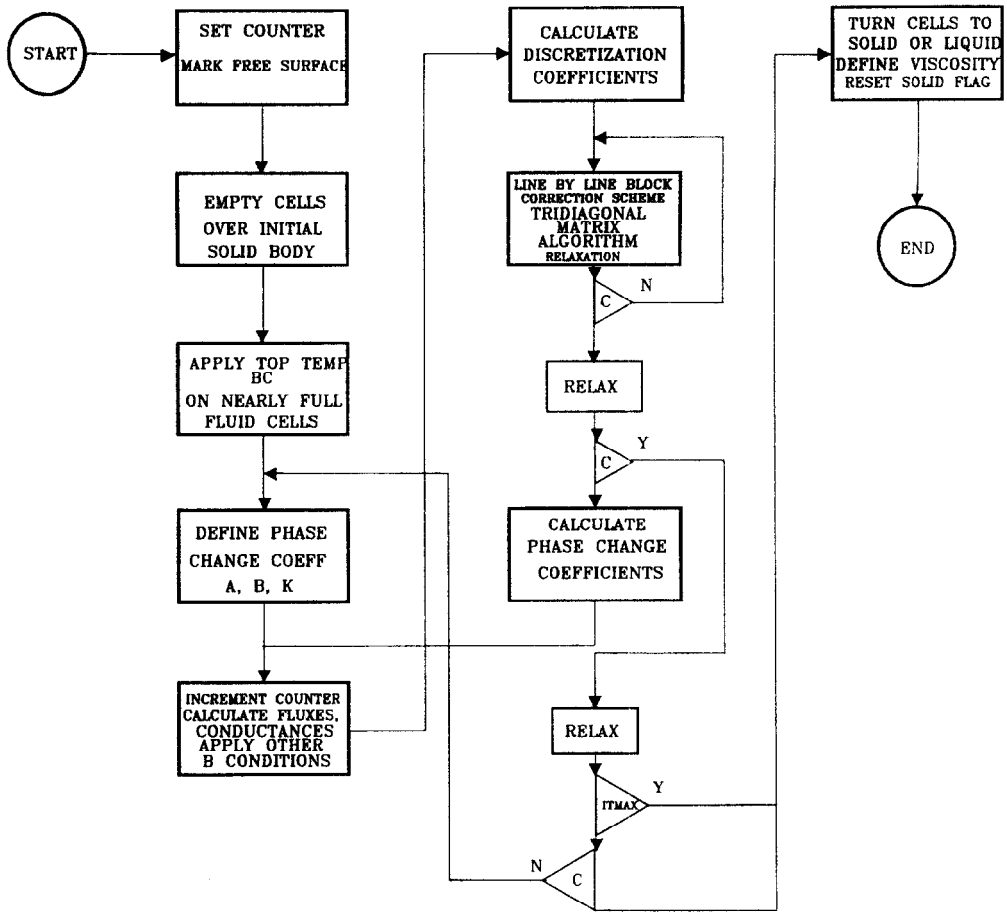

Fig. 4. Flow chart for the temperature algorithm: this algorithm uses the control volume finite difference approach.

of fluid method will use this viscosity to calculate the velocity components in the subsequent time step.

3. RESULTS AND DISCUSSION

The FORTRAN computer program [12] was extensively modified, compiled and executed on a SUN SPARC station 20. It took 91 h to generate 281 μs of real time laser drilling data. It was observed that most of the time was spent in the implicit solution algorithm of the phase-change submodel where under-relaxation of the variables were required in addition to conforming to several fine, strict tolerances. This could not be circumvented due to the nonlinear nature of the solution.

The time sequence of solid contours at selected time intervals shown in Fig. 5 depicts the solid material that is left behind after drilling where the molten material is removed by melt ejection. Alternatively, it can be said the contours show the advancement of the melt–solid interface in to the metal with time. At time zero, the solid consists of 100 cells in the radial direction and 25 cells in the axial direction. Each cell is 5.08 μm by 5.08 μm square in real space. There are 25 empty cells on top of the solid cells. The diameter of the laser beam is 508 μm which is also the extent of the solid in the radial direction. The solid cell is marked in the program with a flag whose value is set to -1. Figure 6 shows vividly the radial movement of the fluid (melt) due to the radial impressed pressure gradient as seen in Fig. 7. Temperature contours shown in Fig. 8 illustrate the shallow penetration of the melt–solid interface (corresponds to nondimensionalized temperature 0) as drilling proceeds due to removal of melt. Finally, the velocity vectors shown in Fig. 9 portray the relative magnitude of the vectors in the thin melt layer. It can be observed that the velocity is zero on the melt–solid interface and is the highest at the outer edge where ejection takes place. The contours and the vectors are available at every 10 μs, enabling us to make an animation of the drilling process. It is clear more material is removed at the center along the axis and as one proceeds radially outward less and less material is removed. This behavior is in good order with the laser beam intensity profile, temperature and pressure profiles which are maximum along the axis and decrease with radius in a Gaussian manner. The stair case effect seen in the solid material is mainly due to the coarseness of the grid that resulted due to the trade-off between the mesh density and the solution time. The contours and the vectors are shown for the

test case where the maximum laser intensity I_0, is 1 MW/cm^2. The laser intensity I varies both as a function of time and space in a Gaussian fashion [13]. This means the material removal rate (g/s), will vary with time, a small number at the beginning, reach a maximum and then diminish. However, the average material removal rate, i.e. the material removed per second can be compared with the experimentally observed result to assess the validity of the numerical model. Nd-YAG laser of 400 W power rating was used at the Pratt and Whitney drilling facility to drill holes in Hastelloy-X material, the thermophysical properties of which at elevated temperatures are not available fully [13] to be used in the numerical simulation. However, this problem was overcome by using the properties of Superalloy [14] which are more or less closer to that of Hastelloy-X. The material removal rates were calculated from the numerical simulations at 1, 3.2 and 5.4 MW/cm^2, respectively. Using the solid contour plots at two different time steps, namely for the 5.4 MW/cm^2 case, at 69 and 108 μs, respectively, a graphical integration was performed to calculate the material removed which was then divided by the time interval of 39 μs to arrive at the material removal rate of about 1 g/s. For the 1 MW/cm^2 case, using 100 and 211 μs data, it was calculated as 0.69 g/s. The experimental material removal rate for the 5.4 MW/cm^2 case was 0.92 g/s [13] which was obtained by scaling a micrograph of a single shot drilled hole for 700 μs at the Pratt and Whitney drilling facility.

The previous comparison between the numerical and experimental data was obtained at 5.4 MW/cm^2 peak intensity, using a switch-on switch-off phase-change model where the simulation ran only for 15 μs and underpredicted the experimental result by about 20%. The new improved model, however, overpredicts the experimental observation by about 10% only. This is a very good agreement considering the uncertainties in the properties, laser beam profile etc. One of the uncertainties associated with the numerical simulation is the way the heat flux decreases and hence the temperature boundary condition, on the top surface, from the edge of the laser beam away to the outer boundary in the increasing radial direction. In the simulation discussed, by observing the solid contours, it looks as though the temperature is brought down very slowly allowing more material to be removed. This probably explains the overprediction. It should be mentioned, however, that the material removal due to vaporization and sublimation damage is not accounted for yet. Nonetheless, the results are very encouraging and there are many ways the model could be improved which will form the basis for further research in this area of laser material processing.

4. CLOSURE

The numerical simulation strategy and the results obtained for the generalized thermal laser drilling model are presented. This has resulted in a significantly improved version of our previous model where the melting and solidification submodel used a crude switch-on switch-off technique. A robust temperature transforming model previously tested with experiments and analytical solutions using a fixed grid methodology in Cartesian coordinates has been modified to deal with a cylindrical coordinate system and tested with available results in the literature. The quantitative agreement has been found to be very good. After verification, it is incorporated in to the laser drilling model to simulate laser drilling process for different laser intensity levels. Time evolution contours and velocity vectors are shown for a test case. Comparison with experimental data in terms of material removal rates is very encouraging, closer than we predicted before and paves the way for further research.

Table 1. Laser drilling material removal rates: comparison between simulation and experiment

I_0MW/cm^2	Pulse (μs)	Removal rates (g/s)	Data source
1.0	50	0.33	N (previous)
1.0	210	0.69	N (present)
3.2	25	0.44	N (previous)
3.2	147	0.87	N (present)
5.4	15	0.73	N (previous)
5.4	210	1.0	N (present)
5.4	700	0.92	E

REFERENCES

1. Nichols, B. D., Hirt, C. W. and Hotchkiss, R. S., *SOLA-VOF: A Solution Algorithm for Transient Fluid Flow with Multiple Free Boundaries*. Los Alamos Scientific Laboratory, LA-8355, 1980.
2. Patankar, S. V., *Numerical Heat Transfer and Fluid Flow*. McGraw-Hill, New York, 1980.
3. Patankar, S. V., *Computation of Conduction and Duct Flow Heat Transfer*. Innovative Research Inc., MN, 1991, pp. 70–72, 323–329.
4. Cao, Y., Faghri, A. and Chang, W. S., A temperature transforming model with a fixed grid numerical methodology for phase-change problems including natural convection. *National Heat Transfer Conference*, HTD-Vol. 109, 1989, pp. 45–53.
5. Voller, V. R., Cross, M. and Markatos, N. C., An enthalpy method for convection/diffusion phase change. *International Journal for Numerical Methods in Engineering*, 1987, **23**, 271–284.
6. Voller, V. R. and Prakash, C., A fixed grid numerical methodology for convection–diffusion mushy region phase-change problems. *International Journal of Heat and Mass Transfer*, 1987, **30**(8), 1709–1718.
7. Morgan, K., A numerical analysis of freezing and melting with convection. *Computer Methods in Applied Mechanics and Engineering*, 1981, 275–284.
8. Sparrow, E. M., Ramsey, J. W. and Kemink, R. G., Freezing controlled by natural convection. *ASME Journal of Heat Transfer*, 1979, **101**, 578–584.

9. Humphries, W. R. and Griggs, E. I., A design handbook for phase change thermal control and energy storage devices. NASA Technical Paper 1074, 1977.
10. Griggs, E. I. and Yarbrough, D. W., Thermal Conductivity of Solid Unbranched Alkanes from n-Hexadecane to n-Eicosane. *Proceedings*, 14*th Southeastern Seminar on Thermal Sciences*, 1978, pp. 256–267.
11. Beilstein, F. K., *Beilstein's Handbook for Organic Chemistry*. First Set, Vol. 4, 1958, p. 563.
12. Ganesh, R. K., Bowley, W. W., Bellantone, R. and Hahn, Y., A model for laser hole drilling in metals. *Journal of Computational Physics*, 1996, **125,** 161–176.
13. Bellantone, R., Ganesh, R. K., Hahn, Y. and Bowley, W. W., A model of laser hole drilling: calculation with experimental comparison. *Proceedings of the* 10*th International Invitational Symposium on the Unification of Numerical, Analytical & Experimental Methods*, WPI, Worcester, MA 01609, 1991, pp. 317–339.
14. Chan, C. L. and Mazumder, J., One-dimensional and steady-state model for damage by vaporization and liquid expulsion due to laser-material interaction. *Journal of Applied Physics*, 1987, 4583.